JTE HCM-UTE
ISSN: 2615-9740

JOURNAL OF TECHNICAL EDUCATION SCIENCE
Ho Chi Minh City University of Technology and Engineering
Website: https://jte.edu.vn
Email: jte@hcmute.edu.vn

Facile Chemical Reduction Synthesis of Cu/Cu_2O Nanostructures: From Spherical Nanoparticles to Anisotropic Nanorods

Thi Phuong Nhi Le[+], Duy Nguyen Nguyen[+], Minh Tien Le, Trung Thach, Thuy Quang Ma, Thi Thu Ha Le, Hai Dang Ngo, Thi Kim Hang Pham[*]
Ho Chi Minh City University of Technology and Engineering, Vietnam

[*]Corresponding author. Email: hangptk@hcmute.edu.vn
[+]These authors contributed equally to this work

ARTICLE INFO

Received: 16/09/2026
Revised: 01/10/2026
Accepted: 14/10/2026
Online First: 11/11/2026
Published:

KEYWORDS

Copper nanostructure;
Chemical reduction;
Core-shell;
Localised surface plasmon resonance;
Sodium borohydride.

ABSTRACT

Copper nanostructures are promising inexpensive substitutes for noble-metal nanomaterials. However, controlling their phase purity and morphology is challenging due to the facile oxidation of metallic copper during synthesis and storage. In this work, the effect of the amount of reducing agent on the phase composition and morphology of the copper nanostructures prepared by chemical reduction was investigated. Four samples (M1–M4) were obtained from $CuCl_2.2H_2O$ in ethanol with sodium borohydride volumes of 0.2–0.8 mL, with polyvinylpyrrolidone added after the main reduction step as the stabilizer, and characterized by X-ray diffraction, scanning electron microscopy and ultraviolet–visible spectroscopy. The diffraction patterns reveal only the face-centered cubic Cu phase at low reducing agent amounts and a dominant Cu_2O phase at high reducing agent amounts. Electron micrographs reveal the evolution of the morphology from irregular aggregated particles, to the coexistence of spheres and nanorods up to about 1.3 µm long, to agglomerated spheres at the highest content. All the samples exhibit a localized surface plasmon resonance band that red-shifts from ~630–640 nm (M1, M2) to ~650–670 nm (M3, M4), indicating that metallic Cu is retained in all samples, plausibly as a Cu core covered by a Cu_2O surface layer. Thus, the amount of reducing agent controls the phase composition and the growth mode, offering a simple route to tune copper nanostructures for catalytic, sensing and conductive-ink applications.

DOI: https://doi.org/10.54644/jte.2026.2600

Copyright © JTE. This is an open access article distributed under the terms and conditions of the Creative Commons Attribution-NonCommercial 4.0 International License which permits unrestricted use, distribution, and reproduction in any medium for non-commercial purpose, provided the original work is properly cited.

1. Introduction

For recent decades, nanotechnology has been presented as an interdisciplinary research field for the synthesis and fabrication of new materials with nanometer-size structures and useful properties, attracting the interest of many scientists in the world [1], [2]. Nanomaterials are materials consisting of at least one dimension in the range of 1 nm to 100 nm [1], [3]. When the size of the material is reduced to the nanometer scale, the higher surface area will significantly increase the physical and chemical properties of the material, which leads to pronounced size and surface effects and changes in quantum and plasmon effects [2], [4], [5]. Due to this increase, nanomaterials have potential applications to help produce commercial products with optimized mass, size, function, and performance, such as foldable screen smartphones, catalyst layers in fuel cells for electric vehicles, supercapacitors with extremely fast charge and discharge capabilities, and medical applications such as nanorobots that help detect and mark disease-causing molecules in the human body; transport and distribute drugs to cancer cells; biosensors that detect disease-causing viruses, toxic gas sensors in the environment, and pesticide residue detection in agricultural products [6]–[13].

Those prominent characteristics have led to extensive investigations of nanomaterials, such as inorganic materials, organic materials and organic-inorganic hybrid materials [14]. The controlled design and synthesis of metal nanomaterials with specific size, morphology, composition and structure

have become an important research direction among inorganic materials, because these materials combine the characteristic properties of the metals and the effects that appear only at the nanometer scale [14], [15]. Metal nanoparticles typically have a larger specific surface area and higher surface energy than bulk metal materials, which leads to stronger interactions with light and electrons [16], [17]. Metallic nanomaterials including gold (Au), silver (Ag), copper (Cu) and platinum (Pt) have been extensively investigated for applications in medicine, electronics, catalysis, biosensors, environmental remediation and energy conversion [18]–[25].

Copper nanoparticles are one of the metallic nanomaterials that have a lot of potential for applications due to the balance between efficiency and cost of manufacture. Copper is one of the most abundant metals in the Earth's crust. The average copper content in the continental crust is about 27 ppm, in the oceanic crust it is 78 ppm, and in the soil it is about 39 ppm. It is inexpensive with rich raw materials. Copper is also a metal with high electrical conductivity and very high thermal conductivity of about 399 W/m. K [26]. The copper nanoparticles prepared at the nanometer scale not only retain the inherent properties of metallic copper but also show many excellent properties due to the effect of particle size and large surface area. Particularly, copper nanoparticles are able to absorb light through the phenomenon of localized surface plasmon resonance (LSPR), to generate characteristic optical properties [27]. In addition, this material exhibits high catalytic activity, good antibacterial properties and excellent electrical conductivity, which provides a basis for broad applications in the preparation of conductive inks, electrodes, sensors, catalytic materials, batteries and functional coatings. Due to these advantages, copper nanoparticles are becoming one of the most active researched and developing materials in the domain of modern materials science [28]–[33].

Despite having many advantages, there are many challenges in the fabrication of copper nanoparticles. During the synthesis and storage process, copper nanoparticles are very easy to agglomerate and oxidize when exposed to oxygen and moisture in the air [34]. This oxidation process could lead to the formation of Cu_2O or CuO phases on the surface of the particles, changing the crystal structure, phase composition, optical properties, electrical conductivity, and catalytic activity of the material [34], [35]. Also, the synthesis conditions such as the type of precursor, reducing agent, stabilizer, temperature, pH, reaction time and synthesis environment have strong influence on the size, shape, crystallinity and particle size distribution [35]–[37]. Therefore, a control of these parameters is important for the synthesis of high quality and stable copper nanoparticles.

At present, copper nanoparticles can be synthesized by different methods such as thermal reduction, ultrasonic reduction, chemical reduction, thermal decomposition, laser ablation, electron beam irradiation, polyol, etc [38]–[40]. Each method has its pros and cons in terms of reaction conditions, control over morphology, particle size, purity and manufacturing costs. Among them, the chemical reduction method is one of the most popular methods due to its simple implementation process, no need for overly complex equipment, the ability to synthesize at relatively low temperatures, and the ease of adjusting reaction parameters to control the size and morphology of the nanoparticles. However, the structural and property characteristics of copper nanoparticles should be investigated as an indispensable requirement for the full assessment of the material quality after the synthesis. The material's crystal structure, phase composition, morphology, particle size and optical properties are determined by common techniques such as X-ray diffraction (XRD), scanning electron microscopy (SEM) and ultraviolet-visible absorption spectroscopy (UV-Vis). These characterization methods allow us to elucidate the relationship between the synthesis conditions and the structure and properties of copper nanoparticles, and provide a basis for guiding appropriate applications.

Considering the problems discussed above, the present work was carried out to synthesize copper nanomaterials using suitable methods as well as to study the structural, morphological and optical properties of the materials after the synthesis. The samples of copper nano were analyzed by appropriate characterization techniques for evaluation of their crystal structure, phase composition, size, particle shape and optical properties, which enabled us to clarify the influence of the synthesis conditions on the characteristics of the material. The research results not only provide the scientific basis for the synthesis and quality control of copper nanoparticles, but also provide a good reference for the development and application of materials in electronics, catalysis, sensor, energy, environmental treatment and

antibacterial materials. Against a background of increasing demand for high-performance, cost-effective and environmentally friendly functional materials, research and investigation of copper nanoparticles remain a scientifically and practically significant direction. Unlike most previous studies, which used a capping agent from the beginning of the reaction [41]–[43], this work introduced PVP only after the main reduction stage, while varying the amount of $NaBH_4$ at a fixed amount of copper precursor. This approach allows the combined effect of reduction kinetics and unprotected early-stage growth on the phase composition (Cu versus Cu_2O) and on the formation of rod-like structures to be assessed using a simple, low-cost, one-pot procedure in air.

2. Materials and Methods

2.1. Chemicals

The following chemicals are used in the chemical reduction synthesis of copper nanoparticles: $CuCl_2.2H_2O$, $NaBH_4$, Polyvinyl pyrrolidone (PVP), ethanol 99.7%. All syntheses were carried out in air, without an inert atmosphere. The detailed synthesis steps are as follows:

2.2. Synthesis of copper nanostructures

Step 1: Stock solutions were prepared separately in ethanol under magnetic stirring. Specifically, 0.0486 g of $CuCl_2.2H_2O$ was dissolved in ethanol to obtain a Cu^{2+} precursor solution with a concentration of approximately 19 mM. The $NaBH_4$ solution was freshly prepared immediately before use, while the PVP solution was prepared separately at a concentration of 37.5–38.5 mM. To maintain the desired $NaBH_4{}^{2+}$ molar ratios of 1.70, 1.75, 1.80, and 1.85 for samples M1–M4, respectively, the $NaBH_4$ concentrations were individually adjusted for each sample.

Step 2: 5 mL of the $CuCl_2 \cdot 2H_2O$ solution and X mL of the $NaBH_4$ solution (X = 0.2, 0.4, 0.6 and 0.8 mL for M1–M4, Table 1) were added to the reaction vessel, and the mixture was stirred with a magnetic stir bar at and 60°C.

Step 3: After 1 h 30 min of reaction, 5 mL of the PVP solution was added to the reaction vessel, and stirring was continued. PVP was intentionally added after the main reduction step so that the nucleation and initial growth of Cu proceeded without a capping agent. Control experiments with PVP present from the beginning of the reaction were not performed in this study.

Step 4: The product was cooled for 30 minutes, and then wash by centrifugation at 3000 rpm (10 minutes, twice times) to obtain the final colloidal solution product.

Table 1. *Amount of $NaBH_4$ used for each sample.*

Sample	Volume of $NaBH_4$ solution (mL)
M1	0.2
M2	0.4
M3	0.6
M4	0.8

2.3. Characterization

The phase composition of the samples was characterized using a D2 PHASER X-ray diffractometer (Bruker, Germany) with Cu Kα radiation (λ = 1.5406 Å). The diffraction patterns were recorded over a 2θ range of 35°–60°, with a step size of 0.02°. The samples were prepared by drop-casting the colloidal suspension onto glass slides, followed by drying to form thin films.

The surface morphology and particle size of the samples were investigated using a field-emission scanning electron microscope (FE-SEM, Hitachi S-4800) operated at an accelerating voltage of 10 kV. For SEM analysis, the copper colloidal suspension was drop-cast onto carbon adhesive tape and dried to form a thin deposit. The particle and nanostructure dimensions, as well as the particle counts, were analyzed using ImageJ software.

The optical properties of the copper colloidal suspensions were measured using a JASCO V-730 UV–Vis spectrophotometer. Before measurement, the colloidal suspension was diluted with ethanol at a volume ratio of 1:10 (colloidal suspension). The diluted samples were transferred into a quartz cuvette with an optical path length of 10 mm (10 × 10 mm). Pure ethanol was used as the reference for baseline correction.

The average crystallite size was estimated using the Debye–Scherrer equation:

$$D = \frac{K\lambda}{\beta cos\theta} \quad (1)$$

where D is the average crystallite size (nm), K is the Scherrer shape factor (typically taken as 0.9), λ is the X-ray wavelength (0.15406 nm for Cu Kα radiation), β is the full width at half maximum (FWHM) of the diffraction peak corrected for instrumental broadening (in radians), and θ is the Bragg diffraction angle.

To account for instrumental broadening, the observed FWHM β_{obs} was corrected using the instrumental FWHM β_{inst} determined from a standard reference material measured under identical instrumental conditions. For diffraction peaks exhibiting Gaussian profiles, the corrected peak broadening β was calculated as:

$$\beta = \sqrt{\beta^2{}_{obs} - \beta^2{}_{inst}} \quad (2)$$

The corrected FWHM was subsequently converted from degrees to radians before being substituted into the Scherrer equation. The instrumental broadening was evaluated as a function of the diffraction angle 2θ to ensure appropriate correction for each diffraction peak.

The calculated crystallite size represents the average dimension of coherently diffracting crystalline domains rather than the physical particle size.

3. Results and Discussion

3.1. Phase composition of the products

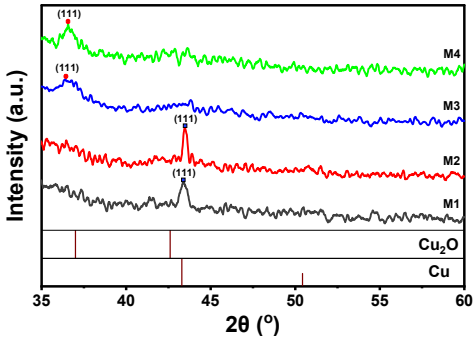


Figure 1. *XRD patterns of the samples change according to the concentration of the reducing agent (M1, M2, M3, and M4).*

Table 2. *Derived parameters of the (111) diffraction peak of Cu (M1, M2) and Cu_2O (M3, M4). Crystallite sizes were estimated using the Scherrer equation (K = 0.9, λ = 1.5406 Å) without correction for instrumental broadening.*

Sample	(h k l)	2θ (°)	FWHM (°)	Grain size (nm)	Lattice spacing d (Å)
M1	(1 1 1)	43.406	0.613	13.942	2.083
M2	(1 1 1)	43.489	0.432	19.896	2.079
M3	(1 1 1)	36.419	2.439	3.425	2.464
M4	(1 1 1)	36.571	0.146	57.284	2.455

The X-ray diffraction (XRD) patterns of the copper nano samples prepared at different concentrations of the reducing agent $NaBH_4$ (M1–M4) are shown in Figure 1 and crystallographic parameters in Table 2. The characteristic diffraction peaks appear at about $2\theta = 43.3^0$ for the (111) crystal plane of Cu with face-centered cubic (FCC) structure which is in accordance with the JCPDS standard card 04-0836. In the spectra of M1 and M2, only the characteristic peaks of metallic Cu are present and no other impurity peaks are observed. The low intensity and broadening of the peaks indicate nanosized crystallites with limited crystallinity. Diffraction peaks at about $2\theta = 36.4^0$ are observed for M3 and M4. These peaks are assigned to the (111) plane of cubic cuprite Cu_2O (JCPDS 34-1354). Thus, the XRD results show that the phase composition of the material can be adjusted by changing the concentration of the reducing agent $NaBH_4$. M1 and M2 show the formation of metallic Cu, while Cu_2O is the dominant crystalline phase in M3 and M4. The peak intensity is still weak and broad, indicating that the formed Cu nanoparticles have low crystallinity, which is consistent with the reduction mechanism of low concentration of $NaBH_4$: the reduction rate of $Cu^{2+} \rightarrow Cu^0$ is slow, and the nucleation process is slow and uneven, so the crystal growth is incomplete.

The XRD patterns show that, as the amount of $NaBH_4$ increases (samples M3 and M4), new diffraction peaks appear at $2\theta \approx 36.4°$. The formation of this oxide phase can be reasonably explained based on the experiment procedure. For high concentration of reducing agent, the rate of the reduction reaction is increased significantly, which results in a higher density of instant crystal nuclei formation (burst nucleation) that leads to a smaller particle size and a larger specific surface area. Significantly, PVP, which acts as a protective/stabilizing agent on the particle surface, is added only in step 3, i.e., after 1 hour and 30 minutes of the main reduction reaction. In the nucleation and initial particle growth stage (step 2), the surface of Cu particles is not yet coated by PVP, leading to the oxidation of smaller particles (in M3, M4) on the surface by dissolved oxygen in the solution or during the centrifugation/washing process (step 4), resulting in the formation of a Cu_2O layer. In M1, M2 the reduction rate is slower so the particles are larger, with a lower surface area/concentration ratio leading to lower sensitivity to oxidation and thus the metallic Cu phase is preserved. Note that the Scherrer crystallite size corresponds to the size of the coherently diffracting domains and not the geometrical dimensions of the particles or rods observed by SEM. Therefore, the very small crystallite size of M3 (~3.4 nm), although the rods are up to ~1.3 μm long (Figure 2), implies that these rods are polycrystalline, meaning they are made up of many small, poorly coherent Cu_2O domains, which is consistent with the oriented attachment of unprotected primary particles prior to the addition of PVP. Conversely, the considerably narrower Cu_2O (111) peak of M4 (FWHM = 0.146^0) indicates much larger coherent domains, which can be attributed to recrystallization and coarsening of the aggregated near-spherical particles at the highest $NaBH_4$ amount. However, this width is close to the instrumental broadening, which was not taken into account, and the value of ~57 nm should be treated only as a rough estimate from below.

Therefore, the XRD results suggest that the concentration of $NaBH_4$ not only affects the crystallinity but also determines the phase composition of the final product, through the nucleation kinetic mechanism and the surface oxidation sensitivity of the particles related with the timing of adding the protective agent PVP into the reaction system.

3.2. Surface morphology of the products

The phase composition data obtained from XRD were complemented with the structural morphology study of the copper nano samples using SEM images (Figure 2) to elucidate the morphological modifications in relation to the concentration of the reducing agent $NaBH_4$.

At the lowest reducing agent concentration (M1), the particles exhibit irregular shapes and tend to aggregate into small clusters, although the boundaries of some individual particles remain recognizable. The particle size distribution appears relatively broad, indicating limited morphological uniformity. These observations are consistent with the XRD results, suggesting that the slow and non-uniform nucleation process at low reducing agent concentrations may contribute to low crystallinity and low morphological uniformity.

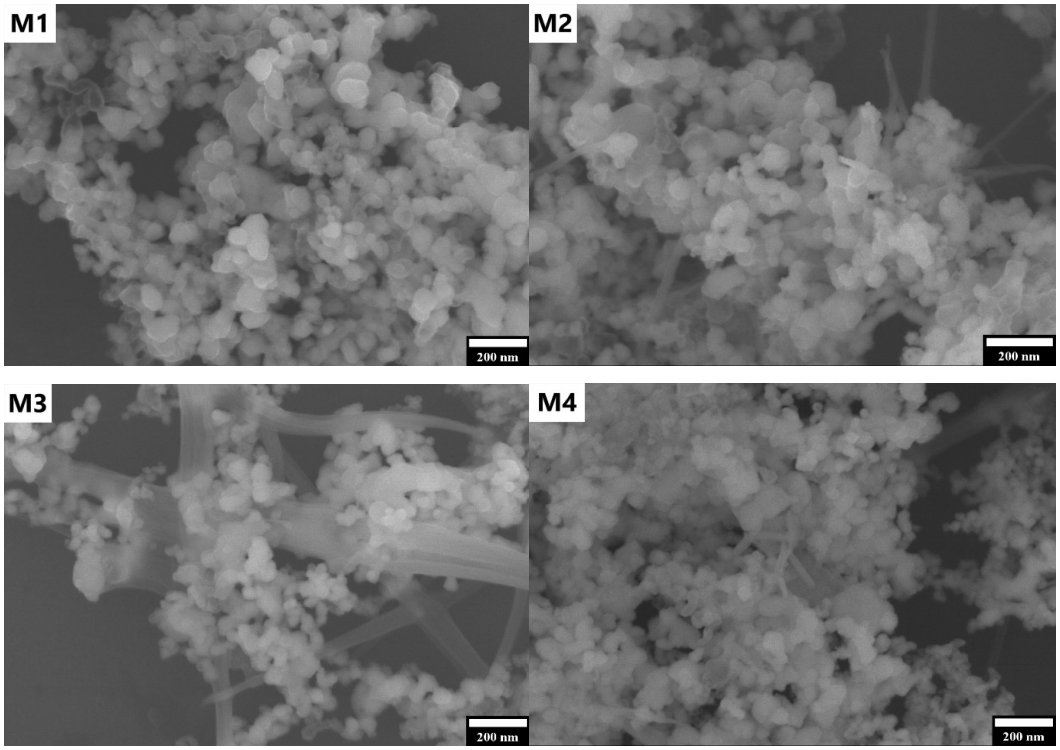


Figure 2. *SEM images of the samples with different concentrations of the reducing agent (M1, M2, M3 and M4).*

With the increase of the reducing agent concentration (M2), the spherical-like nanoparticles become dominant, but some rod-like ones (average length ≈ 330 nm, average diameter ≈ 30 nm) begin to appear intermittently, showing that the increased reduction rate has partially promoted the anisotropic growth of some particles into rod shapes, besides the isotropic growth mechanism forming spherical particles. The trend of developing nanorods can be seen clearly in sample M3. The observed nanorods are sharper and the length and diameter of the rods has increased significantly when compared to M2. The largest rod has a length of 1.3 µm and a diameter of 107 nm and the other rods have lengths over 700 nm and diameters over 50 nm. The phenomenon of uneven particles and agglomeration is still present. The XRD results (Cu_2O appears in M3) suggest that, at this amount of $NaBH_4$, faster surface oxidation of the Cu particles may have favored anisotropic growth along preferred crystal planes, leading to rod-like Cu_2O structures. The dimensions reported in this section are representative values measured on typical SEM fields rather than statistically determined size or aspect-ratio distributions.

For the highest reduction concentration (M4), however, this trend is not observed: The sample shows only nearly spherical particles with uneven sizes and a strong tendency to agglomerate, with almost no Cu or Cu_2O nanowires seen. The disappearance of the rod structure at the highest reduction concentration can be understood in terms of the extremely fast reduction/oxidation rate leading to simultaneous burst nucleation with a very high density so that the time and space for the anisotropic growth of the crystals are limited; thus the particles are prone to isotropic growth (spherical form) and aggregation instead of long rods.

Thus, the SEM results suggest that the $NaBH_4$ concentration controls both phase composition (Cu → Cu_2O, XRD) and mechanism of particle morphology development - from agglomeration of small non-uniform particles (M1) to coexistence of spherical and nanorods particles (M2, M3 - maximum rod size achieved at M3) and then return to agglomerated spherical form in case of too high concentration of reducer (M4).

3.3. Optical properties of the products

The XRD pattern was observed to determine the phase composition. The SEM images were observed to investigate the surface morphology. The UV-Vis spectrum was used to further confirm the successful synthesis of copper nanoparticles with the presence of surface plasmon resonance peaks that are in agreement with the XRD pattern and SEM images provided.

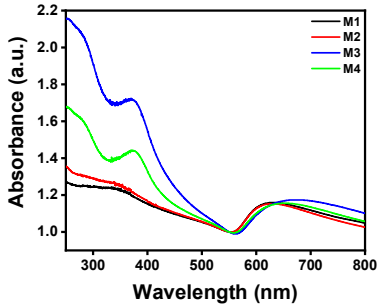


Figure 3. *UV-Vis spectra of the samples depending on the reducing agent concentration (M1, M2, M3, and M4) at wavelengths 250-800nm.*

Figure 3 shows the UV–Vis absorption spectra of samples M1, M2, M3 and M4 investigated in the wavelength range of 250–800 nm for evaluation of the optical properties and electronic transitions of copper. The result indicates that all the samples exhibit strong absorption in the ultraviolet region and gradually decrease when transferred to the visible region. However, the absorption intensity between the samples shows a significant difference, reflecting changes in the electronic structure and the interaction capability with light of each sample.

The absorption intensity of all the samples decreases sharply in the wavelength range of about 400-555 nm and reaches a minimum around 555–560 nm, which corresponds to the transition region between the ultraviolet absorption (interband electronic transition) and the visible region. The absorption spectrum increases again after this, reaching a maximum in the range of 630-670 nm, due to the phenomenon of LSPR characteristic of copper nanoparticles, which is analyzed in detail in Figure 4. Among the samples surveyed, the maximum absorption intensity at the plasmon peak region was observed in M3 and the minimum intensity was observed over the majority of the spectrum in M1, which reflects the differences in the density and morphology of the nanoparticles/nanorods formed at each reducing agent concentration and is consistent with the SEM results presented above.

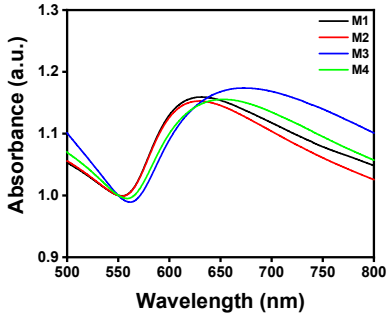


Figure 4. *UV-Vis spectra of samples as a function of reducing agent concentration (M1, M2, M3 and M4) at 500-800nm.*

The UV-Vis absorption spectra of the samples show a common minimum at around 555-560 nm (consistent with the observation in Figure 3) in the wavelength range of 500-800 nm (Figure 4), followed by an increase and the formation of a characteristic absorption band due to the localized surface plasmon resonance (LSPR) phenomenon of free electrons on the surface of copper nanoparticles and nanorods. The LSPR peaks for M1 and M2 are found in the shorter wavelength region (around 630-640 nm), but

M3 and M4 show a strong red-shift with peaks at around 665-670 nm (M3) and 650-660 nm (M4), respectively. A plasmon band is observed in all the four samples indicating the existence of metallic Cu in the entire series including M3 and M4 which are mainly characterized by Cu_2O in the XRD results. Such co-existence is consistent with a metal Cu core covered by a Cu_2O layer in the outside, where the Cu core is responsible for the LSPR signal and the oxide layer with higher refractive index causes the redshift of the resonance. Nevertheless, without TEM/HRTEM, XPS and SAED data, the core–shell configuration is still a plausible hypothesis rather than a confirmed structure. We cannot exclude the possibility of a physical mixture of Cu and Cu_2O particles or partial oxidation of metallic Cu. It is essential to highlight that the interband absorption of Cu_2O (band gap ≈ 2.1-2.2 eV) predominantly takes place below approximately 590 nm. While it may influence absorption in the shorter-wavelength spectrum, it is unlikely to explain the 630–670 nm range. As for the intensity, it is necessary to distinguish by spectral regions: in the resonance peak region (650-700 nm), M3 achieves the highest absorption intensity (~1.17-1.18), higher than M4 (~1.16) and M1, M2 (~1.14-1.15), consistent with SEM results that M3 has the most developed nanorod density. However, this trend is reversed in the longer wavelength range (750-800 nm), where M4 shows the highest absorption intensity (~1.10), M3 the fastest decrease and M2 the lowest (~1.02). This means that despite the highest peak of M3, the absorption range is relatively narrow while M4 has a wider and "flatter" absorption range toward longer wavelengths. The redshift and broadening of the absorption band with increasing reducing agent concentration (from M1/M2 to M3/M4) may be attributed to three contributing factors: (i) the formation of a Cu_2O shell around the Cu core, which modifies the local dielectric environment at the particle surface [44]; (ii) variations in particle/rod size and morphology across the samples, as observed by SEM [45], [46]; and (iii) the relatively broad and non-uniform particle size distribution, which can contribute to LSPR band broadening rather than the formation of a narrow, sharp peak [47].

Systematic information on phase composition, morphology, particle size and optical properties of the copper nanomaterial will be obtained depending on the chosen analytical techniques. By the results of the analysis we can get a clear idea of the process of formation of the material and simultaneously assess the relationship of the conditions of synthesis with the structural characteristics and properties of copper nanoparticles. This provides an important basis for discussing possible applications of the material. This study has several limitations. The coexistence of Cu and Cu_2O was inferred from XRD and UV–Vis data without TEM, XPS or SAED confirmation; the effect of delayed PVP addition was not verified by control experiments: particle and rod sizes were taken from representative SEM images without statistical analysis. The colloidal stability and functional properties of the products were not evaluated. These aspects will be addressed in future work.

4. Conclusions

In this work, copper nanomaterials were successfully synthesized by a chemical reduction method in the presence of different concentrations of the reducing agent $NaBH_4$ to study the effect of synthesis conditions on the structure and properties of the materials. The copper nanoparticles obtained were characterized after synthesis using XRD, SEM and UV-Vis techniques to determine the phase composition, surface morphology and optical properties.

XRD data show that the product is mainly composed of Cu metal phase at low concentrations of the reducing agent. With the increase of $NaBH_4$ concentration, the sample begins to show the presence of Cu_2O phase. This demonstrates that the synthesis conditions directly affect the formation and oxidation process of the material. The SEM results indicate a significant change in morphology with the reducing agent concentration. In the samples M2 and M3 the spherical particles and the rod-like structures are observed simultaneously. The nanorods are most developed in M3. However, when the reducing agent concentration is increased to sample M4, the rod-like structure almost disappears and near spherical particles with uneven size and strong agglomeration are observed instead. Thus, the concentration of NaBH4 not only influences the phase composition but also governs the nucleation mechanism and the morphology development of the material.

The UV–Vis spectrum results recorded the appearance of the localized surface plasmon resonance band characteristic of copper nanoparticles in all samples, confirming the formation of the metallic Cu

phase after the synthesis process. At the same time, the shift of the absorption peak toward the long wavelength and the change of the absorption intensity with the increase of the reducing agent concentration indicate the change of the size, morphology and surface state of the nanoparticles, which is in line with the results obtained from XRD and SEM analysis. The coexistence of the Cu LSPR band and the Cu_2O diffraction peaks suggests a Cu core covered by a Cu_2O surface layer, although direct structural confirmation is still required. The research has indicated that the phase composition, morphology and optical properties of copper nanoparticles are largely dependent on the concentration of reducing agent $NaBH_4$. The obtained results provide a basis for the selection of appropriate fabrication conditions to guide the application of copper nanoparticles and contribute to clarifying the relationship between the synthesis conditions and the material characteristics.

Acknowledgments

This work belongs to the project grant No: SV2026-64 funded by Ho Chi Minh City University of Technology and Engineering, Vietnam.

Conflict of Interest

The authors declare no conflict of interest.

Declaration of generative AI and AI-assisted technologies in the writing process

During the preparation of this work, the authors used Chat-GPT for editing in the English language. The authors reviewed and edited the content as needed and take full responsibility for the content of the publication after using this tool.

Data Availability Statement

The data that support the findings of this study are available from the corresponding author upon reasonable request.

REFERENCES

[1] A. Bratovcic, "Different applications of nanomaterials and their impact on the environment," *SSRG International Journal of Material Science and Engineering*, vol. 5, no. 1, pp. 1–7, Jan.–Apr. 2019.
[2] V. Pokropivny et al., *Introduction to Nanomaterials and Nanotechnology*. Tartu, Estonia: University of Tartu, 2007.
[3] N. Baig et al., "Nanomaterials: A review of synthesis methods, properties, recent progress, and challenges," *Materials Advances*, vol. 2, no. 6, pp. 1821–1871, Jan. 2021, doi: 10.1039/d0ma00807a.
[4] L. H. Madkour, "Introduction to Nanotechnology (NT) and Nanomaterials (NMs)," in *Nanoelectronic Materials: Fundamentals and Applications*, ser. Advanced Structured Materials, vol. 116, Cham, Switzerland: Springer, 2019, pp. 1–47, doi: 10.1007/978-3-030-21621-4_1.
[5] H. Duan et al., "Recent progress and challenges in plasmonic nanomaterials," *Nanotechnology Reviews*, vol. 11, no. 1, pp. 846–873, Jan. 2022, doi: 10.1515/ntrev-2022-0039.
[6] T. Wilberforce et al., "Developments of electric cars and fuel cell hydrogen electric cars," *International Journal of Hydrogen Energy*, vol. 42, no. 40, pp. 25695–25734, Aug. 2017, doi: 10.1016/j.ijhydene.2017.07.054.
[7] M. Sarno, "Nanotechnology in energy storage: The supercapacitors," in *Studies in Surface Science and Catalysis*, A. Basile, G. Centi, M. De Falco, and G. Iaquaniello, Eds., vol. 179. Amsterdam, The Netherlands: Elsevier, 2020, pp. 431–458, doi: 10.1016/B978-0-444-64337-7.00022-7.
[8] S. Alagappan, "Role of nanotechnology in smart phone," *Everyman's Science*, vol. 56, nos. 5–6, Jul. 2023, doi: 10.59094/emsj.v56i5-6.70.
[9] B. Zhang et al., "Recent progress in dielectric/metal/dielectric electrodes for foldable light-emitting devices," *Nanotechnology Reviews*, vol. 12, no. 1, 2023, doi: 10.1515/ntrev-2023-0578.
[10] A. Haleem et al., "Applications of nanotechnology in medical field: A brief review," *Global Health Journal*, vol. 7, no. 2, pp. 70–77, Feb. 2023, doi: 10.1016/j.glohj.2023.02.008.
[11] S. S. Suri et al., "Nanotechnology-based drug delivery systems," *Journal of Occupational Medicine and Toxicology*, vol. 2, no. 1, Art. no. 16, Dec. 2007, doi: 10.1186/1745-6673-2-16.
[12] O. C. Farokhzad et al., "Impact of nanotechnology on drug delivery," *ACS Nano*, vol. 3, no. 1, pp. 16–20, Jan. 2009, doi: 10.1021/nn900002m.
[13] M. Ramesh et al., "Nanotechnology-enabled biosensors: A review of fundamentals, design principles, materials, and applications," *Biosensors*, vol. 13, no. 1, Art. no. 40, Dec. 2022, doi: 10.3390/bios13010040.
[14] M. Rizwan et al, "Types and classification of nanomaterials," in *Nanomaterials: Synthesis, Characterization, Hazards and Safety*, M. B. Tahir, M. Sagir, and A. M. Asiri, Eds., Micro and Nano Technologies. Amsterdam, The Netherlands: Elsevier, 2021, pp. 31–54, doi: 10.1016/B978-0-12-823823-3.00001-X.
[15] H. Cheng et al., "Syntheses and properties of metal nanomaterials with novel crystal phases," *Advanced Materials*, vol. 30, no. 26, Art. no. e1707189, Apr. 2018, doi: 10.1002/adma.201707189.
[16] E. Roduner, "Size matters: Why nanomaterials are different," *Chemical Society Reviews*, vol. 35, no. 7, p. 583, 2006, doi: 10.1039/b502142c.

[17] S. Linic et al., "Photochemical transformations on plasmonic metal nanoparticles," *Nature Materials*, vol. 14, no. 6, pp. 567–576, May 2015, doi: 10.1038/nmat4281.
[18] H. Daraee et al., "Application of gold nanoparticles in biomedical and drug delivery," *Artificial Cells, Nanomedicine, and Biotechnology*, vol. 44, no. 1, pp. 410–422, 2014, doi: 10.3109/21691401.2014.955107.
[19] X. Luo et al., "Application of nanoparticles in electrochemical sensors and biosensors," *Electroanalysis*, vol. 18, no. 4, pp. 319–326, Jan. 2006, doi: 10.1002/elan.200503415.
[20] H. D. Beyene et al., "Synthesis paradigm and applications of silver nanoparticles (AgNPs): A review," *Sustainable Materials and Technologies*, vol. 13, pp. 18–23, Aug. 2017, doi: 10.1016/j.susmat.2017.08.001.
[21] L. Wei et al., "Silver nanoparticles: Synthesis, properties, and therapeutic applications," *Drug Discovery Today*, vol. 20, no. 5, pp. 595–601, 2015, doi: 10.1016/j.drudis.2014.11.014.
[22] M. Bhagat et al., "Review—Multifunctional copper nanoparticles: Synthesis and applications," *ECS Journal of Solid State Science and Technology*, vol. 10, no. 6, Art. no. 063011, Jun. 2021, doi: 10.1149/2162-8777/ac07f8.
[23] S. A. Kumar et al., "Preparation and characterization of copper nanoparticles/zinc oxide composite modified electrode and its application to glucose sensing," *Materials Science and Engineering C*, vol. 30, no. 1, pp. 86–91, 2010, doi: 10.1016/j.msec.2009.09.001.
[24] H. Yu et al., "Recent progress of the practical applications of the platinum nanoparticle-based electrochemistry biosensors," *Frontiers in Chemistry*, vol. 9, Art. no. 677876, May 2021, doi: 10.3389/fchem.2021.677876.
[25] A. Marinoiu et al., "One-step synthesis of graphene supported platinum nanoparticles as electrocatalyst for PEM fuel cells," *International Journal of Hydrogen Energy*, vol. 46, no. 22, pp. 12242–12253, 2021, doi: 10.1016/j.ijhydene.2020.04.183.
[26] S. M. Kraemer, "Copper," in *Encyclopedia of Geobiology*, J. Reitner and V. Thiel, Eds., Encyclopedia of Earth Sciences Series. Dordrecht, The Netherlands: Springer, 2011, pp. 290–291, doi: 10.1007/978-1-4020-9212-1_61.
[27] F. Eker et al., "A comprehensive review of nanoparticles: From classification to application and toxicity," *Molecules*, vol. 29, no. 15, Art. no. 3482, Jul. 2024, doi: 10.3390/molecules29153482.
[28] K. Venkata Abhina et al, "Copper conductive inks: synthesis and utilization in flexible electronics," *RSC Advances*, vol. 5, pp. 63985–64030, 2015, doi: 10.1039/C5RA08205F.
[29] J. M. Zen et al., "Amino acid analysis using disposable copper nanoparticle plated electrodes," *The Analyst*, vol. 129, no. 9, p. 841, 2004, doi: 10.1039/b401573h.
[30] E. Alzahrani et al., "Synthesis of copper nanoparticles with various sizes and shapes: Application as a superior non-enzymatic sensor and antibacterial agent," *International Journal of Electrochemical Science*, vol. 11, no. 6, pp. 4712–4723, May 2016, doi: 10.20964/2016.06.83.
[31] N. K. Ojha et al., "Copper nanoparticles as inexpensive and efficient catalyst: A valuable contribution in organic synthesis," *Coordination Chemistry Reviews*, vol. 353, pp. 1–57, Oct. 2017, doi: 10.1016/j.ccr.2017.10.004.
[32] P. Han et al., "Copper nanoparticle-incorporated carbon fibers as free-standing anodes for lithium-ion batteries," *Nanoscale Research Letters*, vol. 11, no. 1, Art. no. 172, Mar. 2016, doi: 10.1186/s11671-016-1389-6.
[33] T. Kruk et al., "Nanocomposite multifunctional polyelectrolyte thin films with copper nanoparticles as the antimicrobial coatings," *Colloids and Surfaces B: Biointerfaces*, vol. 181, pp. 112–118, 2019, doi: 10.1016/j.colsurfb.2019.05.014.
[34] M. El Zowalaty et al., "Synthesis, characterization, and antimicrobial properties of copper nanoparticles," *International Journal of Nanomedicine*, vol. 8, p. 4467, Nov. 2013, doi: 10.2147/ijn.s50837.
[35] D. Mott et al., "Synthesis of size-controlled and shaped copper nanoparticles," *Langmuir*, vol. 23, no. 10, pp. 5740–5745, Apr. 2007, doi: 10.1021/la0635092.
[36] J. Wang et al., "Synthesis of copper nanoparticles with controllable crystallinity and their photothermal property," *Colloids and Surfaces A: Physicochemical and Engineering Aspects*, vol. 626, Art. no. 126970, Jun. 2021, doi: 10.1016/j.colsurfa.2021.126970.
[37] S. V. Gudkov et al., "Influence of the concentration of Fe and Cu nanoparticles on the dynamics of the size distribution of nanoparticles," *Frontiers in Physics*, vol. 8, Nov. 2020, doi: 10.3389/fphy.2020.622551.
[38] N. A. Dhas et al., "Synthesis, characterization, and properties of metallic copper nanoparticles," *Chemistry of Materials*, vol. 10, no. 5, pp. 1446–1452, Apr. 1998, doi: 10.1021/cm9708269.
[39] N. S. Powar et al., "Cu nanoparticle: Synthesis, characterization, and application," *Chemical Methodologies*, vol. 3, no. 4, pp. 457–480, Jul. 2019, doi: 10.22034/chemm.2019.154075.1112.
[40] J. Ramyadevi et al., "Synthesis and antimicrobial activity of copper nanoparticles," *Materials Letters*, vol. 71, pp. 114–116, 2012, doi: 10.1016/j.matlet.2011.12.055.
[41] G. Ma *et al.*, "A hydrophobic Cu/Cu_2O sheet catalyst for selective electroreduction of CO to ethanol," *Nature Communications*, vol. 14, no. 1, p. 501, Jan. 2023, doi: 10.1038/s41467-023-36261-1.
[42] H. T. Truong, T. H. T. Pham, and L. Q. Le, "Fast and simplified fabrication of Cu/Cu_2O nanocomposites for antioxidant and antibacterial activities," *Materials Technology*, vol. 39, no. 1, Aug. 2024, doi: 10.1080/10667857.2024.2387454.
[43] Aguilar, R. Esparza, and G. Rosas, "Synthesis of Cu nanoparticles by chemical reduction method," *Transactions of Nonferrous Metals Society of China*, vol. 29, no. 7, pp. 1510–1515, Jul. 2019, doi: 10.1016/s1003-6326(19)65058-2.
[44] M. K. Oh et al., "Multiple surface plasmon resonances in silver and copper nanorods," *Journal of Materials Chemistry*, vol. 21, no. 47, p. 19069, 2011, doi: 10.1039/c1jm13613e.
[45] J. M. J. Santillán et al., "Analysis of the structure, configuration, and sizing of Cu and Cu oxide nanoparticles generated by fs laser ablation of solid target in liquids," *Journal of Applied Physics*, vol. 113, no. 13, Apr. 2013, doi: 10.1063/1.4798387.
[46] I. Yaremchuk et al., "Effect of oxidation of copper nanoparticles on absorption spectra of DLC:Cu nanocomposites," *Diamond and Related Materials*, vol. 99, Art. no. 107538, Nov. 2019, doi: 10.1016/j.diamond.2019.107538.
[47] R. Borah and S. W. Verbruggen, "Effect of size distribution, skewness, and roughness on the optical properties of colloidal plasmonic nanoparticles," *Colloids and Surfaces A: Physicochemical and Engineering Aspects*, vol. 640, Art. no. 128521, Feb. 2022, doi: 10.1016/j.colsurfa.2022.128521.

Thi Phuong Nhi Le is a final-year student in the Faculty of Applied Sciences at Ho Chi Minh University of Technology and Engineering (HCM-UTE), Vietnam, majoring in Materials Technology.
Email: 2313000037@student.hcmute.edu.vn. ORCID: https://orcid.org/0009-0005-9544-0854.

Duy Nguyen Nguyen is a graduate in Materials Technology from the Faculty of Applied Sciences at the Ho Chi Minh City University of Technology and Engineering (HCM-UTE). He is currently a lab technician at the NTT Hi-tech Institute. The in-depth research focuses on the properties of silver and copper nanomaterials.
Email: duynn@ntt.edu.vn. ORCID: https://orcid.org/0009-0004-1136-3947.

Minh Tien Le is a fourth-year student majoring in Materials Technology at the Faculty of Applied Sciences, University of Technology and Engineering, Ho Chi Minh City, Vietnam.
Email: 23130053@student.hcmute.edu.vn. ORCID: https://orcid.org/0009-0002-1705-7196.

Trung Thach received MS. degree in Nuclear and High Energy Physics from Ho Chi Minh City National University, University of Science in 2015. The research focuses on radiation safety, gamma-ray scattering, or nuclear spectroscopy.
Email: thachtrung@hcmute.edu.vn. ORCID: https://orcid.org/0009-0003-1440-5607.

Thuy Quang Ma received her MS. degree in Nuclear and High Energy Physics from Ho Chi Minh City National University, University of Science in 2015. The research focuses on radiation safety, particle physics, or nuclear spectroscopy.
Email: quangmt@hcmute.edu.vn. ORCID: https://orcid.org/0009-0006-3174-2092.

Thi Thu Ha Le received her Master's degree in Nanomaterials and Nanodevices from the VNU University of Engineering and Technology, Vietnam National University, Hanoi, Vietnam. The research interests focus on nanomaterials, nanodevices, and their applications in advanced technologies. Currently, the author serves as a lecturer at Ho Chi Minh City University of Technology and Engineering, Vietnam.
Email: haltt@hcmute.edu.vn. ORCID: https://orcid.org/0009-0003-9209-2722.

Hai Dang Ngo received Ms degree at Ajou university, Suwon, Korea and PhD degree at Hokkaido university, Sapporo, Japan. The interest focuses on optical, electrical properties of thin films and low dimentional systems. Currently, the author serves as a lecturer at Ho Chi Minh City University of Technology and Engineering, Vietnam.
Email: dangnh@hcmute.edu.vn. ORCID: https://orcid.org/0000-0002-6205-0850.

Thi Kim Hang Pham received her MS. degree from the Institute of Physic, Hanoi, Vietnam in 2011 and then achieved a PhD. degree from Ewha University, Korea in 2019. Currently, the author serves as a lecturer at Ho Chi Minh City University of Technology and Engineering, Vietnam. The author has a lot of experience in fabricating and characterizing many magnetic and semiconductor materials using physical deposition techniques.
Email: hangptk@hcmute.edu.vn. ORCID: https://orcid.org/0009-0000-4865-3420.